ACS APPLIED MATERIALS & INTERFACES

RESEARCH ARTICLE

www.acsami.org

Cytotoxicity of Graphene Oxide and Graphene in Human Erythrocytes and Skin Fibroblasts

Ken-Hsuan Liao,[†,‡] Yu-Shen Lin,[‡,§] Christopher W. Macosko,[*,†] and Christy L. Haynes[*,§]

[†]Department of Chemical Engineering and Materials Science and [§]Department of Chemistry, University of Minnesota, Minneapolis, Minnesota 55455, United States

Supporting Information

ABSTRACT: Two-dimensional carbon-based nanomaterials, including graphene oxide and graphene, are potential candidates for biomedical applications such as sensors, cell labeling, bacterial inhibition, and drug delivery. Herein, we explore the biocompatibility of graphene-related materials with controlled physical and chemical properties. The size and extent of exfoliation of graphene oxide sheets was varied by sonication intensity and time. Graphene sheets were obtained from graphene oxide by a simple (hydrazine-free) hydrothermal route. The particle size, morphology, exfoliation extent, oxygen content, and surface charge of graphene oxide and graphene were characterized by wide-angle powder X-ray diffraction, atomic force microscopy, X-ray photoelectron spectroscopy, dynamic light scattering, and zeta-potential. One method of toxicity assessment was based on measurement of the efflux of hemoglobin from suspended red blood cells. At the smallest size, graphene oxide showed the greatest hemolytic activity, whereas aggregated graphene sheets exhibited the lowest hemolytic activity. Coating graphene oxide with chitosan nearly eliminated hemolytic activity. Together, these results demonstrate that particle size, particulate state, and oxygen content/surface charge of graphene have a strong impact on biological/toxicological responses to red blood cells. In addition, the cytotoxicity of graphene oxide and graphene sheets was investigated by measuring mitochondrial activity in adherent human skin fibroblasts using two assays. The methylthiazolyldiphenyl-tetrazolium bromide (MTT) assay, a typical nanotoxicity assay, fails to predict the toxicity of graphene oxide and graphene toxicity because of the spontaneous reduction of MTT by graphene and graphene oxide, resulting in a false positive signal. However, appropriate alternate assessments, using the water-soluble tetrazolium salt (WST-8), trypan blue exclusion, and reactive oxygen species assay reveal that the compacted graphene sheets are more damaging to mammalian fibroblasts than the less densely packed graphene oxide. Clearly, the toxicity of graphene and graphene oxide depends on the exposure environment (i.e., whether or not aggregation occurs) and mode of interaction with cells (i.e., suspension versus adherent cell types).

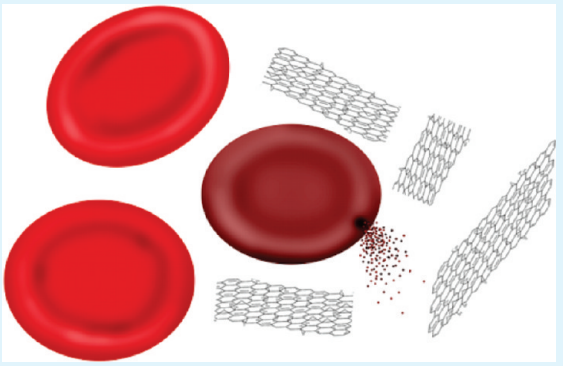

KEYWORDS: graphene, cytotoxicity, hemolysis, aggregation, viability assay

INTRODUCTION

Graphene, a two-dimensional carbon sheet with single-atom thickness, has recently attracted significant interest due to its unique mechanical and electrical properties.[1] This newly discovered material has a wide range of potential applications including transistors,[2] transparent conductors,[3] surfactants,[4] polymer reinforcement,[5] and biodevices.[6] Recently, similar to carbon nanotubes (CNTs), biological applications of graphene sheets (GS) and graphene oxide (GO) have attracted attention in the scientific community based on their great potential for bacterial inhibition,[7] drug delivery,[8] and photothermal therapy.[9] Graphene morphology is distinct from that of CNTs; for example, the length of CNTs influence their toxicity but GS and GO do not have a "length". One similarity between the materials is that both GO/GS[5] and CNT[10] structures vary according to the synthetic processes employed, which can also change their physical properties, such as dispersity, surface functionality, and their toxicity.[11] Several methods have been reported to produce graphene economically.[12,13] The method employed herein starts with exfoliation of graphite oxide to single-layered GO followed by reduction of the GO to GS. GO can be chemically reduced without changing the sheet size because hydroxyl and epoxy groups are converted into carbon−carbon double bonds by dehydration or other reactions.[13,14]

Even with the aforementioned promise of graphene-based materials, there are only a few studies investigating the in vitro cytotoxicity of GO and GS to baterial or mammalian cells, all published in 2010 and 2011.[8,15−19] For toxicity of graphene and its derivatives to bateria, Hu et al. reported that GO and reduced GO (rGO) inhibit bacterial growth with minimal toxicity to human alveolar epithelial A549 cells.[7] Akhaven et al. compared

Received: April 7, 2011
Accepted: June 8, 2011
Published: June 08, 2011

Scheme 1. Sample Preparation Flowchart of Graphene Oxide and Graphene Sheets: GO, bGO, pGO-5, pGO-30, and GS

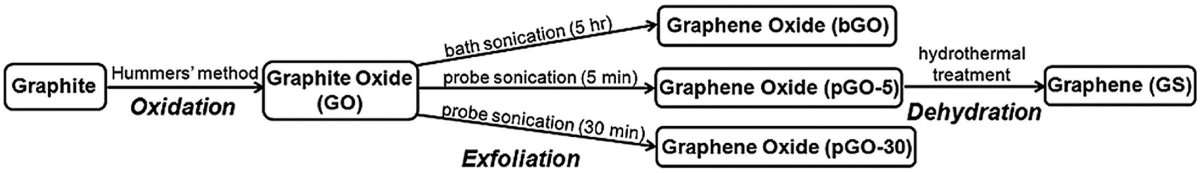

the toxicity of GO and rGO on *Escherichia* and *Staphylococcus* bacteria and found (1) that GO and rGO caused bacterial membrane damage and (2) that the hydrazine-reduced GO was more toxic than untreated GO.[15] They attributed the toxicity of their reduced GO to sharper nanowalls. In the case of cytotoxicity of GO and GS to adherent mammalian cells, Biris and co-workers demonstrated that both GS and CNTs induce cytotoxic effects on phaeochromocytoma (PC-12) cells; they also concluded that the CNTs are more toxic than graphene and that the shape of these carbon-based nanomaterials plays an important role in their cytotoxicity.[16] In very recent work, Wang et al demonstrated that GO has dose-dependent toxicity to human fibroblast cells with the GO causing obvious toxicity when the dose is higher than 50 μg/mL.[17] On the contrary, two other very recent reports show high biocompatibility of GO or GS.[18,19] Ryoo et al reported that GO and GS substrates were highly biocompatible and improved gene transfection efficacy in NIH-3T3 fibroblasts.[18] Chang et al suggested GO will not enter A549 cells and showed no obvious toxicity to A549 cells, regardless of the size or dose of GO.[19] To summarize, the limited published work indicates that both GO and GS have high bacterial toxicity but there is no consensus on cellular toxicity. One likely source of this apparent disagreement is that the physicochemical properties of GO or GS, such as size, surface charge, particulate state, surface functional groups, and residual precursors, are not always well controlled, though they likely have significant influence on biological/toxicological activity.[20] Another possibility is that the most commonly used viability assay, the MTT assay, is not appropriate for work with carbon-based nanomaterials like carbon black and CNTs.[21,22]

To date, the reported literature only probes the in vitro toxicity of GO and GS in bacterial, adherent mammalian, or cancerous cells. Likely because of the recent discovery and progress on graphene, none of this work has investigated and compared the effect of the particulate state of GO and GS on the response of suspended cells like red blood cells and adherent cells like human skin fibroblast cells. In this work, we aim to systematically study the effects of GO exfoliation, size, oxygen content, and particulate state on red blood cells (RBCs), a likely site of interaction for biomedical applications that require intravenous injection, as well as human skin fibroblasts, a likely target upon dermal interaction. RBC toxicity is assessed by tracking hemolysis, or the release of hemoglobin upon cell lysis, under various nanomaterial exposure conditions while fibroblast toxicity is assessed with a comparison between the well-established methylthiazolyldiphenyl-tetrazolium bromide (MTT) and water-soluble tetrazolium salt (WST-8) assays. Together, these data reveal some critical chemical and physical parameters that determine the biocompatibility and promise of these exciting new materials. On the basis of likely broad future use of GO and GS in a variety of products, it is critical to consider cytotoxicity of well-characterized graphene materials on the cell types that are most populous in the body and likely to interact with foreign materials.

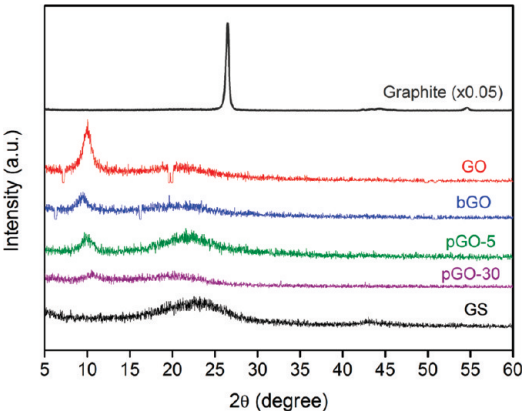

Figure 1. WXRD spectra of (from top) graphite (precursor of GO; gray) as received, graphite oxide (GO; red) as synthesized; graphene oxide (bGO; blue) following 5-h bath-sonication from GO; graphene oxide (pGO-5; green) following 5 min probe-sonication from GO; graphene oxide (pGO-30; purple) following 30 min probe-sonication from GO; and graphene sheets (GS; black) following hydrothermal processing of pGO-5 in D.I. H_2O for 20 h at 130 °C and pH 3.

RESULTS AND DISCUSSION

Synthesis and Characterization of GO and GS. High yields of GO (by Hummers' method[23]) and GS with various sizes, extent of exfoliation and oxygen content were synthesized using a simple aqueous and hydrazine-free hydrothermal route accompanied by different sonication treatments.[13] The sample preparation flowchart is summarized in Scheme 1. The following samples were characterized by wide-angle X-ray diffraction (WXRD) as dried powders: (1) graphite oxide colloidal suspension obtained directly from Hummers' method[23] (GO); (2) graphene oxide obtained after 5 h bath-sonication of GO (bGO), (3) graphene oxide obtained after 5-min probe-sonication of GO (pGO-5), (4) graphene oxide obtained after 30-min probe-sonication of GO (pGO-30), (5) and graphene sheets obtained after hydrothermal processing of pGO-5 in D.I. water for 20 h at 130 °C and pH ~3 (GS). Both bath- and probe-sonication were employed because the differing sonication intensities allowed access to a broad range of material sizes, since the size of GO sheets can be decreased by sonication[5] without influencing the chemical reduction process. To investigate the morphology of the graphene-related materials, WXRD was used. The WXRD (Figure 1) gives the spacing between atomic planes in the main peak: 2θ (Bragg angle) = 10.1° in GO, which corresponds to an interplane distance of d_{0001} = 0.94 nm.[24] In contrast to the WXRD spectrum of GO, the WXRD spectra of bGO, pGO-5 and pGO-30 show

much weaker peaks at $2\theta = 10.1°$, due to the exfoliation of the sheets, a result of long bath-sonication times and powerful probe-sonication. For GS, no peak is observed at $2\theta = 10.1°$ in the WXRD spectrum. The weak broad peak at 23° indicates some stacking of GS.

Atomic force microscopy (AFM) was used to measure the particle size of GO, bGO, pGO-5, pGO-30, and GS. Figure 2a shows GO can reach 10 μm in lateral size and tens of nanometers in thickness (see the Supporting Information (SI), Figure S1). In contrast to GO, micrographs of bGO show that the 5-h bath-sonication significantly exfoliates GO and decreases the particle size (Figure 2b), but multilayer structures are still observed in the AFM images and cross-sectional topography (see the Supporting Information, Figure S1). Figure 2c shows that pGO-5 sheets are smaller than either bGO or GO. The white dotted line in figure 2f is a line scan showing that most of the pGO-5 sheets are approximately 1 nm in thickness, indicating single-layer structures.[25] The

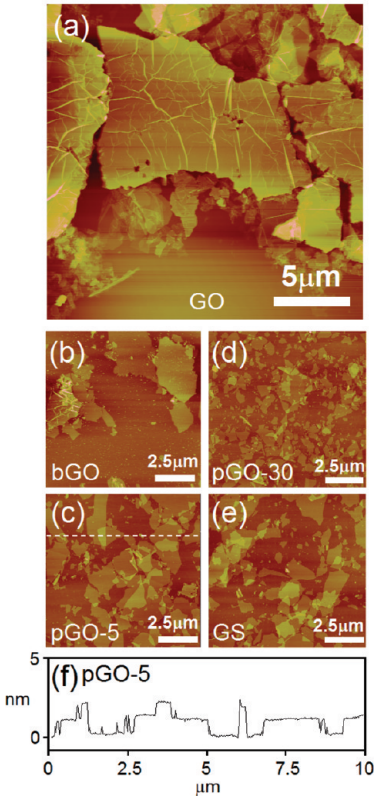

Figure 2. AFM topography images of (a) GO, (b) bGO, (c) pGO-5, (d) pGO-30, (e) GS, and (f) cross-section topography of the white line in c. The cross-sectional topography shows step features of ~1 nm thickness indicating that pGO-5 is mostly single-layered.

AFM images of pGO-30, shown in Figure 2d, reveal that 30-min probe-sonication has broken GO into even smaller pieces than pGO-5, as expected with the longer sonication time. GS was produced via dehydration in an acidic environment[13] from pGO-5 (Scheme 1), and Figure 2e (see the Supporting Information, Figure S1) shows that most of the GS sheets are single-layer with similar size to pGO-5, demonstrating that the hydrothermal process does not significantly affect the particle size. The images in Figure 2 (see the Supporting Information Figure S1) reveal that GS is mostly single-layer after the dehydration reaction; these results are in agreement with previously characterized morphology. In addition, the hydrodynamic diameters of GO, bGO, pGO-5, pGO-30, and GS in D.I. water and PBS as determined by dynamic light scattering (DLS) are listed in Table 1 (hydrodynamic size distribution, see the Supporting Information, Figure S2). Although the DLS characterization can not reveal the exact size of these GO and GS particles in aqueous solution because of the anisotropic morphology of GO and GS, the results still show that the hydrodynamic size of GO decreases in either D.I. water or PBS after intense probe-sonication. Compared to the hydrodynamic diameter of pGO-5, the GS has much larger hydrodynamic diameter, indicating the formation of irreversible aggregates in aqueous solution.

X-ray photoelectron spectroscopy (XPS) was used to measure the chemical composition of GO and GS. Figure 3a shows that the C1s spectrum of GO is an overlap of three peaks at 287.3, 285.6, and 283.5 eV, fingerprints of C═O, C−O and C−C bonds, respectively.[26] XPS measurements performed on GS show a significant drop in C−O character relative to C−C (see Figure 3b). The atomic ratio of oxygen to carbon is reduced from C/O = 2/1 to about C/O = 7/1, which explains the hydrophobic nature of GS and the hydrophilicity of GO sheets. In addition, the oxygen amount in GO and GS also affects their surface charge and dispersity in aqueous solutions.

As mentioned previously, the surface charge[27] and aggregation state[28] of nanomaterials critically influence their in vitro cytotoxicity. The surface charge of nanoparticles plays an especially important role in cell-nanoparticle interactions because cell membranes themselves are charged. In fact, prior to cytotoxicity experiments, characterization of the surface charge and particulate state of the GO and GS samples in biological media is paramount. As shown in Table 1, the zeta (ζ)-potentials of all GO and GS used in this work were negative. The GO samples have similar ζ-potentials in both D.I. water, PBS, and cell culture medium indicating similar oxygen content. Compared to GO, GS has a lower ζ-potential, which is also consistent with the decreased oxygen amount in the XPS data and poor aqueous dispersity.

Although ζ-potential plays a key role in colloidal stability, it does not show the true particulate state in various environments. To estimate the aggregation behavior of GO and GS samples under different aging conditions, we simply used visual evidence

Table 1. GO and GS Characteristics, Values Presented Mean ± Standard Deviation from Triplicate Measurements, Samples Were Measured at 50 μg mL^{-1}

samples	hydrodynamic diameter in D.I. water (nm)	hydrodynamic diameter in PBS (nm)	ζ-potential in D.I. water (mV)	ζ-potential in PBS (mV)	ζ-potential in MEM (mV)
GO	765 ± 19	1678 ± 190	−40.6 ± 2.9	−33.1 ± 1.6	−22.7 ± 0.5
bGO	748 ± 13	1574 ± 160	−40.6 ± 2.2	−31.1 ± 0.8	−23.9 ± 1.7
pGO-5	672 ± 13	1254 ± 143	−41.2 ± 1.3	−31.1 ± 1.9	−23.9 ± 3.3
pGO-30	342 ± 17	861 ± 115	−42.4 ± 2.7	−34.6 ± 1.7	−22.6 ± 0.7
GS	3018 ± 36	4312 ± 206	−37.2 ± 1.6	−24.7 ± 2.6	−17.1 ± 1.4

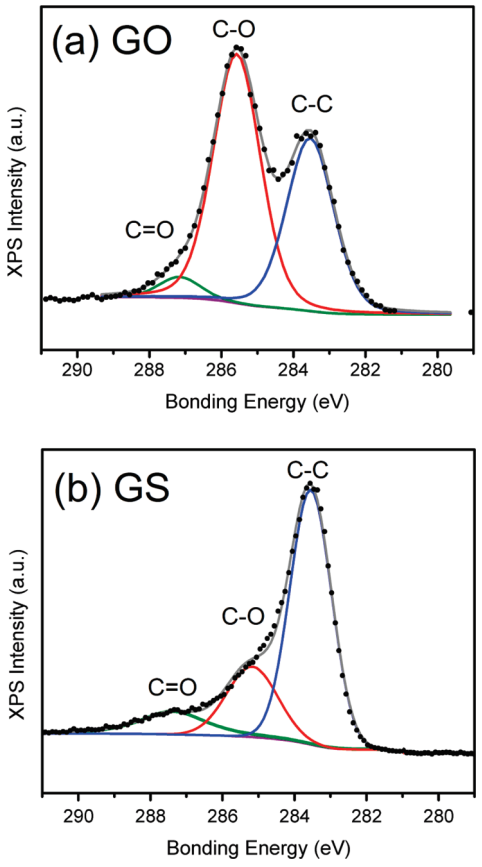

Figure 3. XPS C1s spectra and fitted curves of (a) GO and (b) GS. GS show a significant drop in C−O (285.6 eV; red) character relative to C−C (283.5 eV; blue). The XPS spectra show that there is significant reduction of oxygen from GO (C/O = 2/1) to GS (C/O = 7/1). The purple curve is the fitted baseline.

of settling. The concentration of GO and GS samples used for particle stability in D.I. water and PBS was 50 μg/mL. All the GO samples show excellent colloidal dispersity and stability in D.I. water (see Figure SI S3a−d in the Supporting Information) even after 24 h at 37 °C. We attribute this to their high negative surface charge (electrostatic stabilization). However, even though the surface charge of GS was negative in D.I. water, GS formed observable aggregates and came completely out of suspension after 24-h static aging at 37 °C (see Figure S3d in the Supporting Information), probably due to more $\pi-\pi$ stacking interactions between the deoxygenated surfaces.[29] To study the cytotoxicity of nanomaterials, in most cases, particles will be suspended in highly salted solutions, like phosphate buffered saline (PBS) and culture medium. Accordingly, the colloidal stability of GO and GS was also evaluated in PBS because the results will more accurately model their actual particulate state in toxicity assays and biological environments. In PBS, the GO samples are still homogenously dispersed after 3-h agitation at 37 °C (see Figure S3f in the Supporting Information). However, all the GO samples aggregated after 3 h static aging and completely settled out after 24-h static aging at 37 °C (see Figure S3g,h in the Supporting Information) because of charge neutralization of surface oxygen groups by ionic salt species. In the case of GS, the particles aggregate and settle down to the vial bottom faster in the PBS solution than in D.I. water (see Figure S3c,g in the Supporting Information). In short, GO is highly stable in D.I. water but aggregates in highly salted environments. Importantly, the aggregation of GO can be reversed using external agitation such as mixing or sonication. Compared to the irreversible aggregation of GS, the particulate behavior of GO in highly salted solution is called reversible aggregation in this study.

In vitro Hemolytic Activity of GO and GS. First, the hemolysis assay was employed to evaluate the in vitro blood compatibility of GO and GS because these materials have recently been used for biomedical applications, including injectable graphene-related particles.[8,9] Here, a universal method for testing in vitro nanoparticle hemolysis proposed by McNeil et al[30] was employed to investigate the hemolytic activity of GO and GS. As shown in Figure 4a and b, the membrane of RBCs was compromised by GO and GS in a dose-dependent manner, leading to observable free hemoglobin in the supernatant. The concentrations of GO and GS leading to 50% lysis of RBCs (the TC_{50}) are listed in Table 2. It is apparent that the hemolytic activity of GO increases after sonication, especially for intensely (probe) sonicated GO, like the pGO-5 and pGO-30 samples. The higher hemolytic activity of sonicated GO may be due to the greater extent of exfoliation and smaller GO particle size. The size-dependent cytotoxicity in human RBCs and mammalian cells has also been demonstrated using other types of nanoparticles, such as silica[31,32] and latex.[33] Because GS, compared to all the GO samples, has the lowest oxygen content, it has the lowest hemolytic activity and is also more likely to form aqueous aggregations, yielding fewer cell-contactable reactive oxygen groups on the GS surface. This result is similar to work recently published by Chen and co-workers where the authors found individually dispersed carbon nanotubes were more toxic than aggregated carbon nanotubes.[28] To further study the possible reasons why GO and GS cause hemolysis, hemolysis experiments were performed using graphite (the precursor material for GO and GS). Compared to the high hemolytic activity of GO particles, graphite induces a very low percent hemolysis, even at 200 μg/mL (~3%, see the Supporting Information, Figure S4), most likely due to much lower surface area and hydrophobic surface. This result indicates that the disruption of the RBC membrane is likely attributed to the strong electrostatic interactions between negatively charged oxygen groups on the GO/GS surface and positively charged phosphatidylcholine lipids which are present on the RBC outer membrane.

To confirm that the presence of GO and GS do not interfere the hemolysis measurement method, all particle samples were incubated directly with cell-free hemoglobin (absorbance ~0.88 at 540 nm) for 3 h at 37 °C. The absorbance of the supernatant was compared to a control prepared by high speed centrifugation of pure hemoglobin (see the Supporting Information, Figure S5). The result showed no significant amount of adsorbed hemoglobin on the GO and GS. Additionally, to ensure the UV−vis absorption by GO and GS do not cause overestimation of hemoglobin concentration in the supernatant, all particles suspended in PBS at 100 μg/mL were centrifuged, and the optical density of the supernatant was measured at 540 nm, using 655 nm as reference. The optical densities of all supernatants were very close to background signal, revealing that light absorption by GO and GS is not a significant issue in the hemolysis assay.

Morphological changes and significant lysis of RBCs after GO and GS exposure can be observed by optical microscopy. Compared to the normal biconcave shape of untreated RBCs in PBS (Figure 5a), pGO-5- and pGO-30-treated RBCs (at 25 μg mL^{-1}) appeared in much lower numbers and demonstrate both aberrant morphology and recently lysed RBCs (arrows and circles in the insets of Figure 5 b and c, respectively). Although

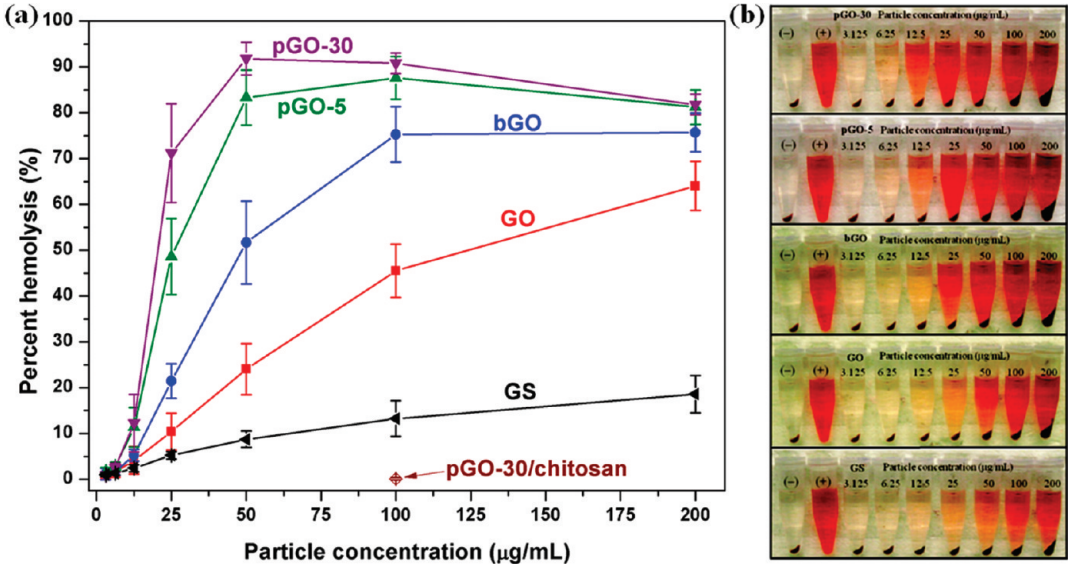

Figure 4. (a) Percent hemolysis of RBCs incubated with different concentrations (3.125 to 200 μg mL^{-1}) of GO (red), bGO (blue), pGO-5 (green), pGO-30 (purple), and GS (black) for 3 h at 37 °C with agitation. Data represent mean ± SD from at least five independent experiments. Also included is the percent hemolysis of RBCs incubated with pGO-30/chitosan at 100 μg mL^{-1} for 3 h at 37 °C with agitation. (b) Photographs of RBCs after 3-h exposure to GO, bGO, pGO-5, pGO-30, and GS at different concentrations (3.125 to 200 μg mL^{-1}). The presence of red hemoglobin in the supernatant indicates RBCs with membrane damage. (+) and (−) symbols represent positive control and negative control, respectively.

Table 2. Concentrations of GO and GS Leading to a 50% Lysis of RBCs

	GO	bGO	pGO-5	pGO-30	GS
TC_{50} (μg mL^{-1})[a]	142	49.6	30.5	20.2	>200

[a] TC_{50} was determined using ED50plus v1.0 free software to fit the data in Figure 4a.

the GS-treated RBCs did not result in significant lysis of RBCs, hemagglutination was observed (arrows in Figure 5d) surrounding the GS aggregates. These data are the first of their kind, systematically studying the hemolytic activity of graphene oxide and graphene sheets toward human RBCs, and it is clear that both particle size and surface charge/oxygen content influence apparent blood compatibility.

To further confirm that the hemolytic activity of these graphene-related particles is attributed to an interaction between RBCs and the GO/GS particle surface, we coated the GO particle with greatest hemolytic activity, pGO-30, with a biocompatible polymer, chitosan, using electrostatic adsorption (for experimental details, see the Supporting Information).[34] The zeta potential of pGO-30/chitosan in acidic water (pH ~4.8) was 24.8 ± 1.8 mV, compared to the zeta potential of pGO-5 in acidic water (−38.3 ± 2.3 mV), indicating that chitosan was successfully coated on pGO-30 surface. However, upon dispersion in PBS (pH~7.4), pGO-30/chitosan aggregates form rapidly due to a pH-dependent chitosan conformational change.[34] Compared to the high hemolytic activity of pGO-30, no apparent hemolysis was observed from pGO-30/chitosan (see Figure 4a and the Supporting Information, Figure S6), revealing that chitosan either serves as a protective layer, masking the electrostatic interactions between RBCs and oxygen groups on the pGO-30 surface, or aggregates the particles to decrease the cell-contactable surface area.

In vitro Fibroblast Cytotoxicity of GO and GS. To further explore the cytotoxicity of GO and GS, two methods, the MTT

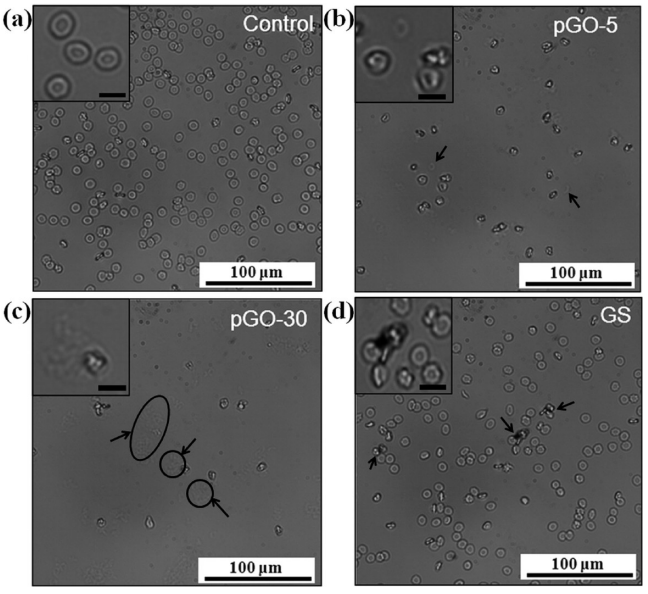

Figure 5. Optical microscographs of RBCs in the presence of (a) PBS (control), (b) pGO-5, (c) pGO-30, and (d) GS at 25 μg mL^{-1} for 3 h at 37 °C with agitation. Inset images are magnified RBCs. Scale bars in the inset images represent 10 μm. The arrows in b and c show lysed RBCs. The arrows in d represent the hemagglutination caused by GS aggregates.

and WST-8 assay, were employed to investigate how these carbon-based nanomaterials interact with adherent cells. In this case, we compare only the cytotoxicity of pGO-5 and GS on mitochondrial activity of human skin fibroblast cells, to focus on the role of oxygen content. The MTT results for both pGO-5 and GS showed no dose-dependent effects on the mitochondrial activity of human skin fibroblast cells (Figure 6), indicating that the adherent fibroblast cells were unaffected by either nanomaterial at any of the employed concentrations. A second

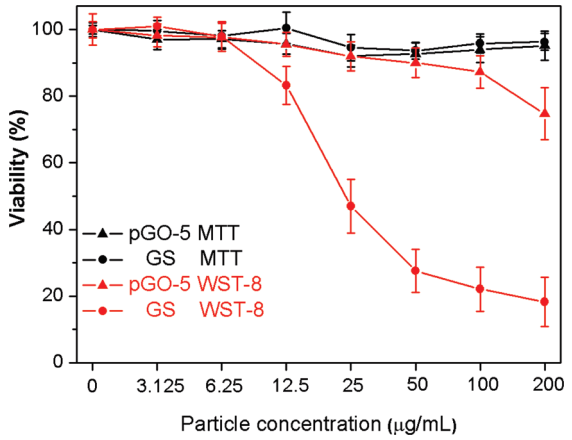

Figure 6. Cell viability of human skin fibroblast cells determined from MTT and WST-8 assay after 24-h exposure to different concentrations of pGO-5 and GS. Data represent mean ± SD.

mitochondrial activity-based assay, WST-8, was employed to verify the MTT result. The WST-8 assay operates on the same principle but uses a negatively charged, water-soluble tetrazolium dye. Compared to the MTT results, WST-8 data showed that both pGO-5 and GS have a dose-dependent effect on the viability of human skin fibroblast cells. There has been previous work done by Monteiro-Riviere et al.[21] and Wörle-Knirsch et al.[22] demonstrating interference by carbon-based materials with the viability marker, MTT reagent, yielding inflated viability results. To rationalize the contradictory results of these two mitochondrial assays with GO and GS particles, control experiments were performed to see if the GO and GS react directly with the MTT or WST-8 reagents, regardless of the state of any cells in the dish. We found that both GO and GS react with MTT to form purple formazan (see the Supporting Information, Figure S7), a result that would indicate viable cells even though there were no cells in this control sample. Marques et al[35] reported a detailed reaction mechanism whereby the [MTT]+ cation can be reduced by electrons and protons, which are present in GS or GO particles (see the Supporting Information, Figure S7). Accordingly, we conclude that the MTT assay is not appropriate for cytotoxicity tests of GO or GS particles. GO and GS particles cause a false positive measure of viability, generating an overestimation of the viability of human skin fibroblasts, especially at high GS and GO doses.

Compared to the MTT control experiment, the WST-8 was not reactive either with GO or GS particles. No detectable reduction of WST-8 (WST-8 formazan formation) occurred after one hour incubation with cell-free GO or GS particles within a wide concentration range (3.125−200 μg mL^{-1}). In addition to the failure of MTT on determining the cytotoxicity of GO and GS, we further found the GO and GS particles adsorbed lactate dehydrogenase (LDH) and generated underestimation of the LDH results (for experimental details, see the Supporting Information). To validate the results of the WST-8 assay, we performed another common viability assay based on trypan blue exclusion. The trypan blue dye exclusion assay shows similar results to those from the WST-8 assay (see the Supporting Information, Figure S8), which confirms the validity of WST-8 assay. In addition, it is clear to see from optical microscopy images (see the Supporting Information, Figure S9) that the fibroblast cell density decreases after 24 h GS exposure at 50 μg mL^{-1}, compared to control and pGO-5 treated cells. These data further confirm the WST-8 results. Accordingly, adherent cell toxicity conclusions will be based on the WST-8 assay results only, indicating that GS is more toxic to adherent cells than pGO-5. This is likely due to the faster sedimentation and formation of more compact aggregates of GS, as compared pGO-5, during 24-h static aging (see the Supporting Information, Figure S3g,h), which greatly inhibits nutrient availability to and growth of human skin fibroblasts. Unlike the hemolysis assay, the human skin fibroblast cells were grown on the bottom of the assay wells, making factors such as the sedimentation rate, thickness and compactness of GO or GS aggregates on the top of adherent cells more likely to affect the viability of fibroblasts. Additionally, the generation of reactive oxygen species (ROS) is a common toxicity mechanism of carbon-based and other nanoscale materials.[36] To investigate this possibility, we performed a ROS assay to measure the oxidative stress generated by pGO-5 or GS particles in or near the human skin fibroblast cells. The results show that the generation of ROS in cells is concentration-dependent after pGO-5 or GS exposure (see the Supporting Information, Figure S10). After 24-h exposure, the aggregated GS at 25 μg mL^{-1} induced approximately a 9-fold increase in ROS in fibroblast cells compared to untreated cells (control). The aggregated GS induced an even higher level of ROS (indicating more oxidative stress) in human skin fibroblast cells compared to reversibly aggregated pGO-5 (see the Supporting Information, Figure S10), revealing a likely mechanism for larger GS toxicity effects compared to pGO-5. This work clearly demonstrates that the particulate state (extent of aggregation, irreversible or reversible aggregation) of GO and GS and the cell types (membrane composition and suspended/adherent nature of cells) used for cytotoxicity evaluation have a great impact on the biological/toxicological responses.

CONCLUSIONS

In this first study of the blood compatibility of graphene-based materials, the blood compatibility and cytotoxicity of graphene oxide (GO) and graphene sheets (GS) of various sizes and oxygen content have been investigated in suspended human RBCs and adherent skin fibroblasts using in vitro hemolysis and WST-8 viability assays. All the GO and GS show dose-dependent hemolytic activity on RBCs. In the case of GO samples, extent of exfoliation and particle size play a critical role in extent of hemolysis. Sonicated (smaller) GO exhibited higher hemolytic activity than untreated (larger) GO. Compared to individually dispersed GO sheets having higher surface oxygen content, the aggregated GS showed lower hemolytic activity. Covering the GO sheets with chitosan eliminated their hemolytic activity.

The spontaneous formation of MTT formazan by cell-free GO and GS indicates the failure of MTT assay in predicting the cytotoxicity of graphene-related materials. The MTT data indicate a false high biocompatibility of GO and GS with adherent fibroblasts. However, the valid WST-8, trypan blue exclusion, and ROS data demonstrate that aggregated GS particles are more cytotoxic than reversibly aggregated GO on human skin fibroblast cells. Moreover, compared to reversibly aggregated GO, the aggregated GS generated more reactive oxygen species in human skin fibroblast cells and strongly associated to the cell surface. Based on the hemolysis and WST-8 viability assay results, this is the first work to show that the particulate state of graphene-based particles has a profound impact on their toxicity to suspended erythrocytes and adherent human skin fibroblasts.

EXPERIMENTAL SECTION

Synthesis of GO and GS. Graphite oxide particle suspension was synthesized using Hummers' method;[23] and a detailed process has been reported in our previous paper.[13] We chose this simple, hydrazine-free method to synthesize graphene oxide and graphene sheets to avoid any unintentional toxicity from the highly toxic hydrazine species. Graphite oxide was dialyzed (Spectrum Laboratories; 5 nm pore size) against deionized (D.I.) water for 48 h. The D.I. water was changed every 4 h. To obtain graphene oxide (GO), graphite oxide was redispersed in D.I. water at 1 wt % concentration and sonicated with a bath-sonicator (Branson 2510; 100 W) or probe-sonicator (Cole Parmer; CPX750, 750W) for various sonication times as described in the Characterization section. GS was produced from pGO-5 using the dehydration process reported in our previous paper.[13] To provide an acid environment for dehydration of hydroxyl groups[8] on pGO-5, HCl was added into the pGO-5/D.I. water solution (1 wt %; yellow solution) until the pH reached ~3. A sealed pressure cooker (PRESTO, 12-Quart) was used to heat the solution to 130 °C for 20 h. The solution turned from homogeneous yellow to a layered suspension with clear water on the top and fluffy black precipitate on the bottom. All the GO and GS samples used for cytotoxicity experiments were dialyzed in regenerated cellulose tubing (with a molecular weight cut off, of 12 000−14 000, Fisherbrand, Pittsburgh, PA) against two liters of D.I. water for at least 6 days. The pH of GO and GS suspensions after dialysis was around 5.

Characterization. *Wide-Angle Powder X-ray Diffraction (WXRD).* GO and GS powders were obtained after drying the aqueous GO and GS suspensions using a rotary evaporator (IKA RV10, Wilmington, NC) equipped with a self-cleaning dry vacuum system (WELCH, Niles, IL). The WXRD measurements for GO and GS were performed on a Bruker-AXS D-5005 (Siemens) with filtered Cu Kα source (2.2 kW) at 45 kV and 40 mA. Data were recorded by step scanning with a step size of 0.040° and a step time of 1.0 s.

Atomic Force Microscopy (AFM). Single drops of GO, bGO, pGO-5, and pGO-30 aqueous suspensions were spin-coated onto separate mica substrates (Ted Pella, Redding, CA) at 4000 rpm for 30 s and air-dried at 45 °C for 3 h. A drop of dispersed GS in cosolvent (10 wt % D.I. water and 90 wt % dimethylformamide) was dropped onto a mica substrate and air-dried at 65 °C for 3 h. Noncontact mode AFM (Digital Instrument, Nanoscope III Multimode AFM) was used for measurements.

X-ray Photoelectron Spectroscopy (XPS). GO, bGO, pGO-5, pGO-30 and GS were dried in a vacuum oven at 65 °C for 3 h before the XPS measurements. The XPS spectra were recorded on a Surface Science SSX-100 spectrometer equipped with a monochromatic Al Kα radiation source.

Dynamic Light Scattering (DLS). The hydrodynamic diameter of GO, bGO, pGO-5, pGO-30 and GS was determined using a 90Plus/BI-MAS particle size analyzer (Brookhaven Instruments Corporation, Holtsville, NY). All the particles were suspended in D.I. water and PBS at a concentration of 50 μg mL^{-1}. Three runs and one minute run duration were set for each measurement. Each measurement was repeated on three cuvettes taken from the same solution.

ζ-Potential Measurements. All GO and GS samples were prepared in D.I. water, PBS, and cell culture medium at a concentration of 50 μg mL^{-1}. ζ-potential was determined using a ZetaPALS Zeta-Potential Analyzer (Brookhaven Instruments Corporation, Holtsville, NY) equipped with a 35 mW red diode laser (660 nm). Five runs and ten cycles were set for each measurement. Each sample was measured at least three times.

Optical Microscopy. Following 3-h exposure to pGO-5, pGO-30, and GS sheets (25 μg mL^{-1}) at 37 °C with agitation, washed RBCs were transferred to a 35 × 10 mm Petri dish (Falcon, Franklin Lakes, NJ) and observed under a Nikon Eclipse TE 2000-U inverted microscope (Nikon USA, Melville, NY). The optical images were recorded using a QUANTEM: 512SC camera (Photometrics, Tucson, AZ) with MetaMorph imaging software (Molecular Devices, Downingtown, PA).

Hemolysis Assay. Fresh ethylenediamine tetraacetic acid (EDTA)-stabilized human whole blood samples were purchased from Memorial Blood Center (St. Paul, MN). Typically, 5 mL of whole blood was added to 10 mL of calcium- and magnesium-free Dulbecco's phosphate buffered saline (PBS, Grand Island, NY) and centrifuged at 500 g for 10 min to isolate RBCs from serum. This purification step was repeated five times, and then the washed RBCs were diluted to 50 mL in PBS. To test the hemolytic activity of GO and GS samples, 0.2 mL of diluted RBC suspension (around 4.5 × 10^8 cells mL^{-1}) was added to 0.8 mL of GO and GS suspension solutions in PBS at different concentrations. The 250 μg mL^{-1} of GO or GS stock solutions in PBS were prepared by adding 0.8 mL of 500 μg mL^{-1} of GO or GS particle solutions in D.I. water to 0.8 mL of 2X PBS solutions. The final concentration of GO and GS ranges from 3.125 to 200 μg mL^{-1}. D.I. water (+RBCs) and PBS (+RBCs) were used as the positive control and negative control, respectively. All the samples were placed on a rocking shaker in an incubator at 37 °C for 3 h. After incubation, the samples were centrifuged at 10,016 g for 3 min. The hemoglobin absorbance in the supernatant was measured at 540 nm, with 655 nm as a reference, using an iMark microplate reader (Bio-Rad, Hercules, CA). Percent hemolysis was calculated using eq 1.

$$\text{percent hemolysis}\ (\%) = \left(\frac{\text{sample abs}_{540-655\ nm} - \text{negative control abs}_{540-655\ nm}}{\text{positive control abs}_{540-655\ nm} - \text{negative control abs}_{540-655\ nm}}\right) \times 100 \quad (1)$$

MTT Viability Assay. Human skin fibroblast cells (CRL-2522) were purchased from American Type Culture Center (Manassas, VA). Typically, 6 × 10^4 cells were seeded in 96-well plates and cultured in Minimum Essential Medium Eagle (MEM, Hyclone, Logan, UT) with Earle's balance salt and L-glutamine, supplemented with 10% fetal bovine serum (FBS, Invitrogen, Grand Island, NY) and 1% penicillin/streptomycin (PS, Invitrogen, Grand Island, NY) at 37 °C under 5% CO_2. After 24 h, the cells were washed with 100 μL of serum-free MEM (1% PS) twice and incubated with 100 μL of different concentrations of pGO-5 and GS suspensions in serum-free MEM (1% PS). The pGO-5 and GS particles used for viability assays were washed with serum-free MEM (1% PS) five times. After 24 h exposure, the cells were washed twice with 100 μL of serum-free MEM and incubated with 100 μL of 0.5 mg/mL methylthiazolyldiphenyl-tetrazolium bromide (MTT, Invitrogen, Eugene, OR) containing media for 2 h at 37 °C under 5% CO_2. Finally, the MTT containing media was removed and the insoluble purple formazan crystals produced by live cells were dissolved in 100 μL of dimethyl sulfoxide (DMSO, Sigma-Aldrich, Milwaukee, WI). The plate was placed on a rocking shaker for at least 20 min and then 80 μL of the purple DMSO solution in each well was transferred to a new 96-well plate, because residual pGO-5 or GS can affect the absorbance values at 570 nm. Optical density of the produced stain was monitored at 570 nm, with 655 nm as a reference, using an iMark microplate reader (Bio-Rad, Hercules, CA). The cell viability was determined by mitochondrial activity, which was calculated using eq 2. Cells without particle exposure were used as control. In addition, cell-free control experiments were performed to see if the GO and GS react directly with the MTT reagents. Typically, pGO-5 and GS particles with different concentration (3.125−200 μg/mL) were suspended in 1 mL of 0.5 mg/mL of MTT solution (in MEM). After 2 h incubation at 37 °C under 5% CO_2, the pGO-5 and GS particles were centrifuged and washed with PBS one time. To see if any insoluble formazan formed during incubation, we added 1 mL of DMSO to redisperse the pelleted particles. The suspended pGO-5 and GS particles were centrifuged again and the optical density of DMSO supernatant at 570 nm (655 nm as reference) was used to see if the MTT reagent reacted with pGO-5 and GS particles.

$$\text{viability from MTT assay}(\%) = \left(\frac{\text{sample abs}_{570-655\ nm}}{\text{control abs}_{570-655\ nm}}\right) \times 100 \quad (2)$$

WST-8 Viability Assay. In addition to the MTT assay, cell viability was measured using a cell counting kit-8 (CCK-8, Dojindo, Rockville, MD). Typically, 6×10^4 cells were seeded in a 96-well plate and cultured in MEM supplemented with 10% FBS and 1% PS at 37 °C under 5% CO_2. After 24 h, the cells were washed with 100 μL of serum-free MEM (1% PS) two times and incubated with 100 μL of different concentrations of pGO-5 and GS suspensions in serum-free MEM (1% PS). After 24-h exposure, the cells were washed twice with serum-free MEM and 15 μL of CCK-8 solution was added to each well containing 100 μL of serum-free MEM. After one hour incubation at 37 °C under 5% CO_2, 80 μL of the mixture was transferred to another 96-well plate, because residual pGO-5 or GS can affect the absorbance values at 450 nm. The absorbance of the mixture solutions was measured at 450 nm with 655 nm as a reference, using an iMark microplate reader. The viability was calculated using eq 3. The cell-free control experiments were performed to see if the GO and GS react directly with the WST-8 reagents. Typically, 100 μL of pGO-5 and GS particles with different concentration (3.125−200 μg/mL) were added to a 96-well plate and 10 μL of WST-8 reagent solution was added to each well; the mixture solution was incubated at 37 °C under 5% CO_2 for 1 h. After incubation, the pGO-5 and GS particles were centrifuged and 50 μL of supernatant was transferred to another 96-well plate. The optical density at 450 nm (655 nm as reference) of each control was used to see if the pGO-5 and GS particles react with WST-8 reagents.

$$\text{viability from WST} - 8 \text{ assay}(\%) = \left(\frac{\text{sample } abs_{450-655nm}}{\text{positive control } abs_{450-655nm}}\right) \times 100 \quad (3)$$

■ ASSOCIATED CONTENT

Supporting Information. AFM images of GO, bGO, pGO-30, and GS with cross-section topography. Photographs of colloidal stability of GO, bGO, pGO-5, pGO-30, and GS in D. I. water and PBS. Percent hemolysis of graphite. Hemoglobin adsorption on GO, bGO, pGO-5, pGO-30, and GS. Percent hemolysis of pGO-30/chitosan. Photographs of MTT formazan (in the DMSO supernatant) produced by pGO-5 and GS particles without any cells present. Viability of human skin fibroblasts after pGO-5 and GS exposure determined by trypan blue exclusion assay. Optical microscopy images of human skin fibroblasts after pGO-5 and GS incubation. ROS generation in human skin fibroblasts by pGO-5 and GS. This material is available free of charge via the Internet at http://pubs.acs.org.

■ AUTHOR INFORMATION

Corresponding Author

*E-mail: chaynes@umn.edu, macosko@umn.edu.

Author Contributions

‡These authors contributed equally to this work.

■ ACKNOWLEDGMENT

This work was funded by grants from the National Science Foundation (NSF, CHE-0645041) and the Abu Dhabi-Minnesota Institute for Research Excellence (ADMIRE); a partnership between the Petroleum Institute of Abu Dhabi and the Department of Chemical Engineering and Materials Science of University of Minnesota. Y.-S. L. acknowledges financial support from the Taiwan Merit Scholarship (NSC-095-SAF-I-564-052-TMS). TEM, AFM, and XRD characterization were carried out in the College of Science and Engineering Characterization Facility, University of Minnesota, which receives partial support from NSF through National Nanotechnology Infrastructure Network.

■ REFERENCES

(1) Geim, A. K.; Novoselov, K. S. *Nat. Mater.* **2007**, *6*, 183–191.
(2) Hernandez, Y.; Nicolosi, V.; Lotya, M.; Blighe, F. M.; Sun, Z.; De, S.; McGovern, I. T.; Holland, B.; Byrne, M.; Gun'Ko, Y. K.; Boland, J. J.; Niraj, P.; Duesberg, G.; Krishnamurthy, S.; Goodhue, R.; Hutchison, J.; Scardaci, V.; Ferrari, A. C.; Coleman, J. N. *Nat. Nanotechnol.* **2008**, *3*, 563–568.
(3) Novoselov, K. S.; Geim, A. K.; Morozov, S. V.; Jiang, D.; Zhang, Y; Dubonos, S. V.; Grigorieva, I. V.; Firsov, A. A. *Science* **2004**, *306*, 666–669.
(4) Kim, J.; Cote, L. J.; Kim, F.; Yuan, W.; Shull, K. R.; Huang, J. *J. Am. Chem. Soc.* **2010**, *132*, 8180–8186.
(5) Kim, H.; Abdala, A. A.; Macosko, C. W. *Macromolecules* **2010**, *43*, 6515–6530.
(6) Mohanty, N.; Berry, V. *Nano Lett.* **2008**, *8*, 4469–4476.
(7) Hu, W.; Peng, C.; Luo, W.; Lv, M.; Li, X.; Li, D.; Huang, Q.; Fan, C. *ACS Nano* **2010**, *4*, 4317–4323.
(8) Sun, X.; Liu, Z.; Welsher, K.; Robinson, J. T.; Goodwin, A.; Zaric, S.; Dai., H. J. *Nano Res.* **2008**, *1*, 203–212.
(9) Yang, K.; Zhang, S.; Zhang, G.; Sun, X.; Lee, S.-T.; Liu, Z. *Nano Lett.* **2010**, *10*, 3318–3323.
(10) Liang, F.; Chen, B. *Curr. Med. Chem.* **2010**, *17*, 10–24.
(11) Pumera, M. *Chem. Asian J.* **2011**, *6*, 340–348.
(12) Li, X. L.; Zhang, G. Y.; Bai, X. D.; Sun, X. M.; Wang, X. R.; Wang, E.; Dai, H. J. *Nat. Nanotechnol.* **2008**, *3*, 538–542.
(13) Liao, K.-H.; Mittal, A.; Bose, S.; Leighton, C.; Mkhoyan, K. A.; Macosko, C. W. *ACS Nano* **2011**, *5*, 1253–1258.
(14) Kim, M. C.; Hwang, G. S.; Ruoff, R. S. *J. Chem. Phys.* **2009**, *131*, 064704.
(15) Akhavan, O.; Ghaderi, E. *ACS Nano* **2010**, *4*, 5731–5736.
(16) Zhang, Y.; Ali, S. F.; Dervishi, E.; Xu, Y.; Li, Z.; Casciano, D.; Biris, A. S. *ACS Nano* **2010**, *4*, 3181–3186.
(17) Wang, K.; Ruan, J.; Song, H.; Zhang J.; Wo, Y.; Cui, D. *Nanoscale Res. Lett.* 2011, *6*:8.
(18) Ryoo, S.-R.; Kim, Y.-K.; Kim, M.-H.; Min, D.-H. *ACS Nano* **2010**, *4*, 6587–6598.
(19) Chang, Y.; Yang, S.-T.; Liu, J.-H.; Dong, E.; Wang, Y.; Cao, A.; Liu, Y.; Wang, H. *Toxicol. Lett.* **2011**, *200*, 201–210.
(20) Gil, P. R.; Oberdörster, G.; Elder, A.; Puntes, V.; Parak, W. J. *ACS Nano* **2010**, *4*, 5527–5531.
(21) Monteiro-Riviere, N. A.; Inman, A. O. *Carbon* **2006**, *44*, 1070–1078.
(22) Wörle-Knirsch, J. M.; Pulskamp, K.; Krug, H. F. *Nano Lett.* **2006**, *6*, 1261–1268.
(23) Hummers, W. S., Jr.; Offeman, R. E. *J. Am. Chem. Soc.* **1958**, *80*, 1339.
(24) Boukhvalov, D. W.; Katsnelson, M. I. *J. Am. Chem. Soc.* **2008**, *130*, 10697–10701.
(25) Mkhoyan, K. A.; Contryman, A. W.; Silcox, J.; Stewart, D. A.; Eda, G.; Mattevi, C.; Miller, S.; Chhowalla, M. *Nano Lett.* **2009**, *9*, 1058–1063.
(26) Mattevi, C.; Eda, G.; Agnoli, S.; Miller, S.; Mkhoyan, K. A.; Celik, O.; Mostrogiovanni, D.; Granozzi, G.; Garfunkel, E.; Chhowalla, M. *Adv. Funct. Mater.* **2009**, *19*, 2577–2583.
(27) Arivizo, R. R.; Miranda, O. R.; Thompson, M. A.; Pabelick, C. M.; Bhattacharya, R.; Robertson, J. D.; Rotello, V. M.; Prakash, Y. S.; Mukherjee, P. *Nano Lett.* **2010**, *10*, 2543–2548.
(28) Liu, S.; Wei, L.; Hao, L.; Fang, N.; Chang, M. W.; Xu, R.; Yang, Y.; Chen, Y. *ACS Nano* **2009**, *3*, 3891–3902.
(29) Li, D.; Müller, M. B.; Gilje, S.; Kaner, R. B.; Wallace, G. G. *Nat. Nanotechnol.* **2008**, *3*, 101–105.

(30) Dobrovolskaia, M. A.; Clogston, J. D.; Neun, B. W.; Hall, J. B.; Patri, A. K.; McNeil, S. E. *Nano Lett.* **2008**, *8*, 2180–2187.
(31) Lin, Y.-S.; Haynes, C. L. *J. Am. Chem. Soc.* **2010**, *132*, 4834–4842.
(32) Napierska, D.; Thomassen, L. C. J.; Rabolli, V.; Lison, D.; Gonzalez, L.; Kirsch-Volders, M.; Martens, J. A.; Hoet, P. H. *Small* **2009**, *5*, 846–853.
(33) Mayer, A.; Vadon, M.; Rinner, B.; Novak, A.; Wintersteiger, R.; Fröhlich, E. *Toxicology* **2009**, *258*, 139–147.
(34) Fang, M.; Long, J.; Zhao, W.; Wang, L.; Chen, G. *Langmuir* **2010**, *26*, 16771–16774.
(35) Marques, E. P.; Zhang, J.; Tse, Y. -H.; Metcalfe, R. A.; Pietro, W. J.; Lever, A. B. P. *J. Electroanal. Chem.* **1995**, *395*, 133–142.
(36) Garza, K. M.; Soto, K. F.; Murr, L. E. *Int. J. Nanomed.* **2008**, *3*, 83–94.